# Effect of main reinforcement on box girder flexural and shear behavior

*Rawa* N. Abood [1], *Huda* M. Mubarak[1], *Yahyia* M. Hameed[1], *Nawras* T. Abdulrazzaq[1], *Khattab* S. Abdul-Razzaq [1]*, *and Baida N. Hasan* [1]

[1] University of Diyala, Department of Civil Engineering, Diyala, 32001, Iraq

**Abstract.** The primary goal of the current study is to determine, in a lab setting, how the main longitudinal reinforcement ratio affects the behavior and load capacity of single-cell box girders made of reinforced concrete. Three specimens were cast and tested, each with a length of 1600 mm, top and bottom slab has a uniform thickness of 50 mm, an upper flange width of 430 mm, a bottom flange width of 300 mm, and a height of 230 mm. The three box girders are reinforced by having three distinct ACI 318–19 reinforcing ratios: the minimum, the maximum, and average of them, i.e., the reinforcing ratios were 0.0033, 0.0184, and 0.00591, respectively. All three specimens were subjected to 2-concentrated forces. For the tested box girders, the cracking load, crack pattern, failure load, deflection, average strain values on the concrete surface, strain values in steel bars, and failure mode were recorded and discussed. Experimental work has proven that increasing the ratio of the main steel reinforcement from minimum to maximum, passing through the average between them, i.e. 79-425%, leads to higher load capacity by about 66.67-99% and midspan deflection decrease by about 28-36%. It was also concluded that steel reinforcement yield occurred at both minimum and average main reinforcement resulting in flexural failure. While at the maximum of the main reinforcement, yield did not urge but rather a failure occurred in another place which is the shear, whose stirrups suffered from yield this time

## 1 INTRODUCTION

The road network's lifeline is the bridge, both in urban and rural areas. As technology has developed quickly, the traditional bridge has been replaced by an inventive, economical structural design. One of these approaches is the concrete box girder [1, 2]. Because they can be built quickly and easily, adjacent precast, prestressed concrete box girders are a good choice for bridges with short, medium or long spans [3, 4]. Typically, the box has a rectangular or trapezoidal cross section. A box girder made of two web plates linked at the top and bottom by common flanges. Box girders can be categorized based on their construction method, use, and forms. There are three variations of box girders that are frequently utilized in real life. It can be built and manufactured using a single cell, double cell or multiple cells [5]. It may be monolithically built with the deck (closed box girder), or the deck can be separately built later (open box girder). The box girder normally contains either pre-stressed concrete, structural steel, or reinforced concrete [6]. Box girder have become widely used in motorway and bridge systems due to their structural effectiveness, enhanced stability, serviceability, cost-effective construction, and attractive aesthetics [7, 8]. Box girder bridges are becoming increasingly common worldwide. Particularly because of their wide bottom flanges, this kind of bridge resists bending very well [9]. For these essential structures, the deflection term has to be accounted. Engineers observing the deflections have frequently been misled by the long-term deflection behavior of long-span box girder bridges. Without accurate calculations, one can even misread the causes of the fast acceleration of deflection and take the wrong remedial measures, overstretching the bridge and perhaps causing serious damage. The longitudinal bending stress distribution is not uniform across the width of wide flange girders. It is typically impossible to precisely calculate using simple beam theory because it remains highest at the edge and decreases in the center [10]

C. Yilmaz, (1975) [11] provided the findings of an examination of how straight rectangular box girders behave before failing when loads are supplied via diaphragms or from the intersection of the web and flange. Material nonlinearities are taken into consideration during the analysis, which depended on the finite element approach. The authors found that box girder stresses and deflections can be evaluated effectively and precisely using this method,

*Corresponding author: dr.khattabsaleem@yahoo.com

besides, that the behavior of box girders under torsion is impacted by the diaphragm's rigidity. In addition, authors found that it is simple to estimate a diaphragm's required thickness or rigidity to maintain cross-sectional shape. Finally, they stated that the geometry and material properties of a box girder can be used to predict its ultimate strength or load carrying capacity.

M. Hassanain, (2002, July) [12] presented a rigorous and methodical approach to the design of adjacent box girder bridges that makes use of mathematical optimization techniques. A design optimization system that can be used to conduct cost-effectiveness studies of the use of high-performance concrete (HPC) and to create preliminary design charts and guidelines in accordance with AASHTO LRFD Specifications is developed through this procedure. An example of an alphabetical design is provided to demonstrate the optimization system's capabilities and application.

Wang et al, (2022) [13] studied a 30-meter-long simply supported prestressed concrete box girder that is under destructive experiment concept. On the basis of the experiment, the finite strip method (FSM) was used to create a nonlinear numerical model. The design was improved through parametric analyses. Authors found that the tested girder's failure mode was a fracture of the prestressing tendon. Concrete had a maximum compressive strain of only 1456 με in the compression zone, which was significantly less than the ultimate compressive strain of 3300 με. As a result, the top flange's concrete was not fully utilized. The girder that was tested had a ductility index of 1.99 and had a maximum deflection of 1/102 of the span length. Consequently, authors realized that the tested girder was ductile. The measured cracking load was 750 kN, or 1.98 times the applied load for the intended bearing capacity at its ultimate state. Additionally, the maximum load measured was 1872 kN, or 2.50 times the cracking load. The tested girder had a sufficient safety margin.

Mohammed et. al. (2019) [14] studied the effect of different ratios of the main longitudinal reinforcement depending on the ACI 318-14 in reinforced concrete conventional beams. In the case of one central concentrated force, when the reinforcement is increased from the minimum to the average (the average of the minimum and the maximum) and then to the maximum, the load capacity increased by 280% and midspan deflection decreased by 33%. In case of 2-concentrated forces and partial uniformly load, the increase in load capacity became 258% and 50%, and the decrease in deflection became 289% and 28%, respectively. The authors also concluded that the main reinforcement ratio directly affects the failure mode, shifting between flexural and shear, i.e. between ductility and brittleness. This is certainly reflected in the number and shape of cracks in addition to the way they spread.

Abdul-Razzaq et. al. (2019) [15] experimentally studied the effect of main reinforcement ratio variation on the behaviour and load capacity of 2-way reinforced concrete slabs. The outcomes of the experimental study demonstrate that raising the ACI 318-14 main reinforcing steel ratio from minimum, average, and then maximum values, also increases the load capacity, while lowering the midspan deflection. In more detail, the load capacity increases by about 156% when the main reinforcing steel ratio is increased from the minimum to the maximum, while the maximum midspan deflection decreases by around 27-52%. It must be pointed out here that changing the percentage of the main reinforcement may not contribute to changing the failure pattern, but it effectively affects the timing of cracks appearance, the method of their distribution, and even their spread as well.

Accordingly, it is not possible to mention all the previous studies related to the current subject, but the ones closest to the topic of the current study were mentioned. That is why, the authors of the current research work did not find any previous literature studying the effect of the main longitudinal reinforcement ratio on the behavior and load capacity of this type of girders. These box girders are built with large spans; therefore, the role of the main longitudinal reinforcement should be studied. In the current research work, three laboratory box girder specimens were cast and tested. The ratio of the main longitudinal steel reinforcement in these three specimens has been varied to be the ACI 318-19 minimum, maximum reinforcement ratios, and the average of them.

## 2. EXPERIMENTAL PROGRAM

Three reinforced concrete box girder specimens are built and tested here. The span length, cross section's details and shear reinforcement are the same for the three specimens. Concrete box girders are different in the area of longitudinal main reinforcement as shown in Figures 1-3. They all have a section height of 230 mm, a section width of 300 mm for lower flange and width of 430 mm for upper flange. Concrete cover is 10 mm. The shear reinforcement in all box girders are Ø10@80mm. The longitudinal main reinforcement in each box girder is 2Ø12mm for minimum reinforcement (the specimen BG-min), 4Ø12mm for average reinforcement (the specimen BG-avr) and 7Ø12mm for maximum reinforcement (the specimen BG-max).

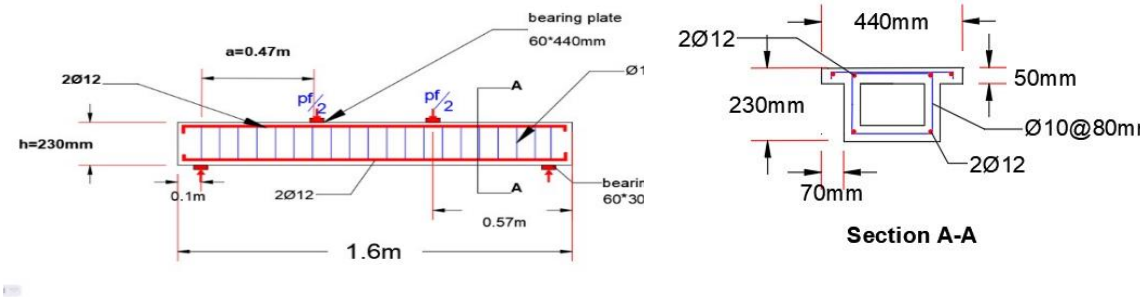


**Fig 1.** Specimen BG–min.

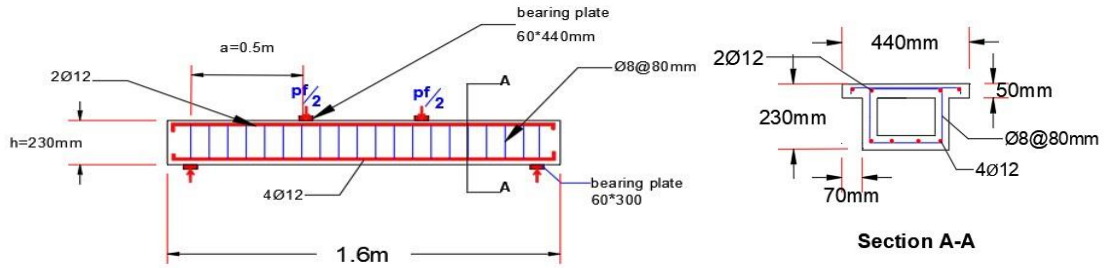


**Fig 2.** Specimen BG–avr

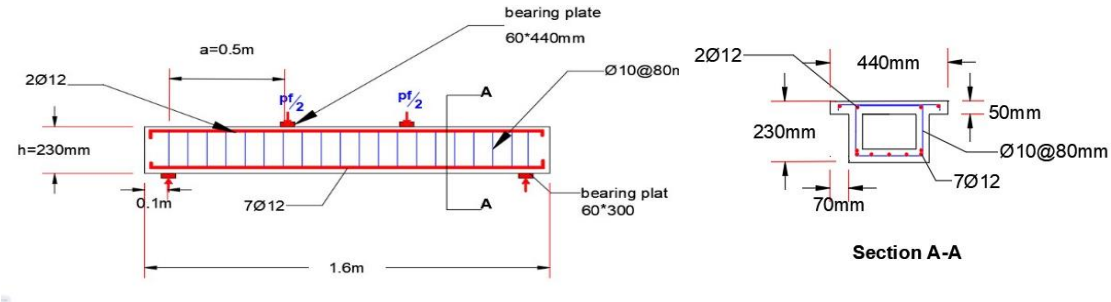


**Fig 3.** Specimen BG–max.

### 2.1. Material Properties of Concrete Box Girders

According to Iraqi Standard Specification I.Q.S. No. 5, 1984 [16], the current study employs regular Portland cement type I from the Tasluja factory. Al-Sudor local graded natural sand with a specific gravity of 2.6 and local crushed gravel with a maximum particle size of 10 mm were utilized in

the concrete compositions. According to the test results, the chosen aggregate complies with Iraqi Specification I.Q.S. No. 45, 1984 [17].

The main reinforcement for the concrete box girders was 2Ø12, 4Ø12 and 7Ø12 deformed steel bars for the specimens BG-min, BG-avr and BG-max, respectively, while deformed steel bars of Ø10@80 mm for shear reinforcement. Table 1 shows the reinforcing steel's mechanical characteristics. The test results show that the adopted steel bars meet the criteria of ASTM A496-02 [18] and ASTM A615/A615M-05 [19].

The three box girder specimens were cast with one concreting campaign that took an entire day, Figure 4. Six 150×300 mm cylinders were cast during the box girder's construction. The splitting tensile strength ($f_{ct}$) of concrete was measured using three cylinders in accordance with ASTM C496-96 [20]. The concrete compressive strength ($f'c$) was measured using the remaining three cylinders in accordance with ASTM C39M-03 [21]. In addition, three 100×100×500 mm prisms were tested to determine the concrete modulus of rapture ($f_r$) in accordance with ASTM C78-02 [22]. All box girder specimens were demolded about 24 hours after casting, then, continuously were covered by a wet thick canvas for 28 days to cure. After 28 days, the box girders were painted to help with the viewing of the test crack. Table 2 summarizes the mix proportions of the concrete components utilized in this investigation, whereas Table 3 presents the attributes of the mixed concrete. The yield stress of the 10 mm bar is 568 MPa and the yield stress of the 12 mm bar is 618 MPa, while the yield strain for them are 0.00273 and 0.00297 respectively.

**TABLE 1.** Mechanical properties of reinforcing steel bars

| Type of used bars | Bar diameter (mm) | Yield stress (MPa) | Yield Strain | Ultimate stress (MPa) |
|---|---|---|---|---|
| Longitudinal main reinforcement | 12 | 618 | 0.00297 | 713 |
| Secondary (Shear) reinforcement | 10 | 568 | 0.00273 | 675 |

**Fig 4-a.** Compressive strength test

**Fig 4-b.** Tensile strength test

**Fig 4-c.** Rapture test

**Fig 4.** Specimen BG–avr

## *2.*2. Test Set-up and Instrumentation

A 600 kN hydraulic universal testing machine from the Jet Materials Ltd Company was used to evaluate the box girders load capacity. To measure mid span deflection, a dial gauge with a 0.01 mm accuracy was installed at the center of the span. In order to determine the strain values in the steel bars and concrete, strain gauges were used in each box girder that was tested. The strain gauges utilized in

the testing program were wire-type BFH120-3AA-X3 with resistances of 120 Ω and sizes of 25×2.3 mm for concrete and 6×2.3 mm for steel reinforcement.

**TABLE 2.** Mix properties of concrete

| Cement content (kg/m$^3$) | Sand content (kg/m$^3$) | Gravel content (kg/m$^3$) | Water content (kg/m$^3$) | Water/cement ratio | Cylinder compressive strength, *f*'c (MPa), 28 days |
|---|---|---|---|---|---|
| 424 | 718 | 715 | 245 | 0.58 | 30.41 |

**TABLE 3.** Characteristics of the concrete used

| Box girder | *f*'c (MPa) | *f*'ct (MPa) | *Ec* (MPa) |
|---|---|---|---|
| BG-min<br>BG-avr<br>BG-max | 30.41 | 3.4 | 25918 |

## 3. RESULS AND DISCUSSIONSTS

As depicted in the Figs 5–7, each box girder was put through a test of increasing static monotonic load until failure. Test load rate was 2 kN/sec. At various loading stages, the outcomes were analyzed and compared. Plotting of the load-deflection responses was done. Initial cracking and failure loads were recorded. After each load increment, the crack propagation, crack patterns and types, steel reinforcement strains, and concrete surface average strains were marked and categorized.

### 3.1 Behavior and Crack Pattern

The experimental test results for the box girder specimens are summarized in Table 4. The diagonal and flexural cracking loads are depicted in Figs 5, 6 and 7, more precisely:

**3.1.1 BG-min:** This box girder specimen experienced a first flexural crack under the applied load at roughly 30% of the experimental failure load (Pf), Fig. 5. A second flexural crack that appeared along the box girder at mid-span was about 40%Pf, and split into two opposite directions occurred as this crack was growing. The shear crack formed about 60%Pf near the supporting zones. Finally, the BG-min specimen failed in ductile flexure. The rapid flexural collapse of the box girder was caused by the first crack, which persisted and spread down the box girder, beneath the location of applied load.
**3.1.2 BG-avr:** It experienced a first flexural crack under the applied load at roughly 16.4%$P_f$, Fig. 6. A second flexural crack appeared along the box girder specimen at mid-span about 24%$P_f$. First shear cracks formed about 48%$P_f$ near the supporting zones. The ductile flexural collapse of BG-avr box girder specimen was caused by the initial crack, which persisted and spread down the box girder, beneath the location of applied load as like as the failure type for specimen BG-min. It is important to note that, in comparison to BG-min, the number of cracks increased with more evenly distribution across the span.
**3.1.3 BG-max:** This box girder specimen experienced a first flexural crack under the applied load at roughly 12.5%$P_f$, Fig. 7. Under the applied load, diagonal cracks began at the face of box girder specimen and spread toward the support around 45%$P_f$. The inclined cracks became wider and continued to spread with additional parallel cracks appearing as a result of increased loading. The secondary web reinforcement (shear reinforcement) yielded when the load reached the failure stage, resulting brittle shear failure.

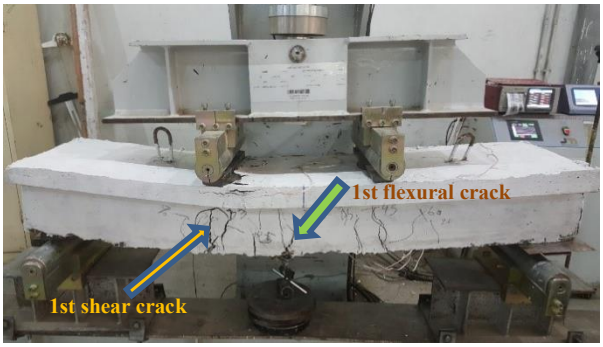


**Fig 5.** BG-min specimen after test

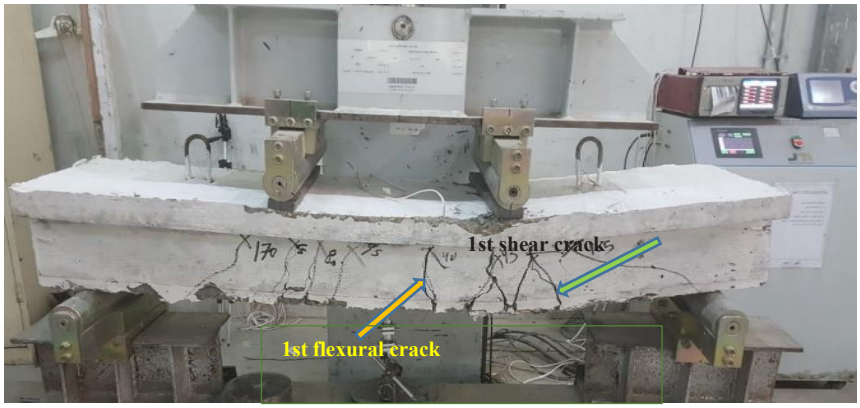


**Fig 6.** BG-avr specimen after test


**Fig 7.** BG-max specimen after test

### 3.2. Load-Deflection Response

Figures 8–10 describe the load-deflection responses based on the amount variation of longitudinal main steel reinforcement. The box girder specimen BG-min, which had ACI 318-19 minimum reinforcing ratios of 0.0033 experienced flexural failure, and BG-avr, which had ACI 318-19 average reinforcing ratios of 0.00591 experienced flexural failure as well. The load-deflection response of the specimen BG-max, which had ACI 318-19 maximum reinforcing ratios of 0.0184, was more brittle than the two other specimens due to its shear failure. Concerning BG-avr, when the main reinforcing ratio was increased, the ductility increase became more apparent. More specifically, an elastic-plastic behavior was more observed in the load-deflection curve for box girder specimen BG-avr. The load-deflection curve indicated that the stiffness increases with increasing reinforcing ratios (ρ), indicating that the change in stiffness occurred prior to cracks becoming visible to the naked eye.

According to the load-deflection response shown in Figs. 8-10, deflection (Δ) decreases as reinforcing ratios (ρ) rises. In comparison with BG-min, the deflection decreased by about 28% and 36% for BG-avr and BG-max, respectively.

To discuss the above, the minimum reinforced beam BG-min, with ρ=0.0033, suffered flexural stresses from the start of loading until failure. This is clearly visible on the load-deflection response shown in Fig. 8, which is characterized by a bowing character. Note that BG-min also contained late shear cracks, but the shear regions (near the supports) were stronger than the flexure region (in the middle of specimen span). As for the beam with average reinforcement BG-avr, ρ=0.00591, it is noted that it suffered from flexural stresses, which overcame the main reinforcement, leading to flexural failure. This beam also contained shear cracks near the supports, and perhaps more obvious than the shear cracks of BG-min, but the failure could not occur at the higher shear regions (near the supports). Accordingly, failure occurred in the middle of the BG-avr span, where the flexural stresses are maximum. This is evident in the load-deflection response shown in Fig. 9.

As for the specimen BG-max, the matter is different, as the main reinforcement was so high (maximum), ρ=0.0184, that it forced failure to occur in the higher shear zones (near the supports), this is evident on the almost straight nature of the load-deflection response shown in Fig. 10. For ease of comparison, Fig. 11 summarizes all the load-deflection relationships for the three different steel ratios of the main reinforcement.

**TABLE 4.** Detailed experimental test results

| Specimen | Reinforcing ratio (ρ) | % Increasing in (ρ) | $f'c$ (MPa) | $P_{cr\text{-}flex}$ (kN) | $P_{cr\text{-}shear}$ (kN) | $P_f$ (kN) | % Increase in $P_f$ | Δ (mm) | % Decrease in Δ | $\Delta_f$ (mm) | Δs (mm) | $P_{cr\,flex}/P_f$ | $P_{cr\,shear}/P_f$ | $\frac{\Delta f}{\Delta}$ | $\frac{\Delta s}{\Delta}$ | Failure type |
|---|---|---|---|---|---|---|---|---|---|---|---|---|---|---|---|---|
| BG1-min | 0.0033 | --- | 31.23 | 30 | 65 | 99 | --- | 32.33 | --- | 11.1 | 24.34 | 0.303 | 0.656 | 0.19 | 0.40 | flexural |
| BG2-ava | 0.00591 | 79 | 30.41 | 27 | 80 | 165 | 66.67 | 23.4325 | 28 | 2.25 | 8.532 | 0.164 | 0.1 | 0.364 | 0.36 | flexural |
| BG3-max | 0.0184 | 457 | 29.51 | 25 | 90 | 199 | 99 | 20.602 | 36 | 2.724 | 7.995 | 0.126 | 0.32 | 0.39 | 0.132 | shear |

where:
$P_f$= final load capacity, $P_{cr\text{-}flex}$=load at 1st flexural crack, $P_{cr\text{-}shear}$=load at 1st shear crack, Δ=maximum midspan deflection, Δs= midspan deflection at 1st shear crack, $\Delta_f$= midspan deflection at 1st flexural crack.

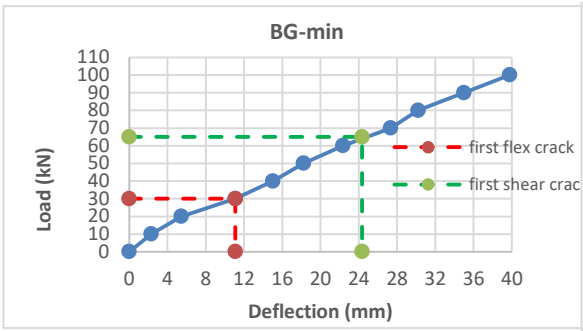


**Fig 8.** Load- deflection curve in mid span for BG-min

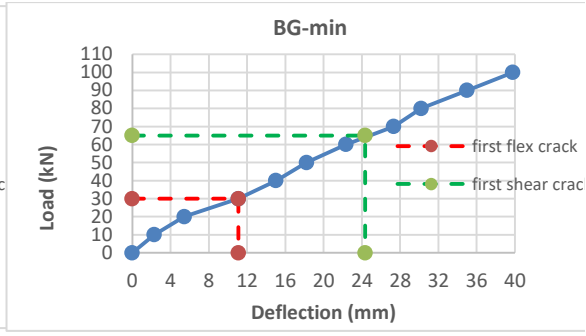


**Fig 9.** load- deflection curve in mid span for BG-avr

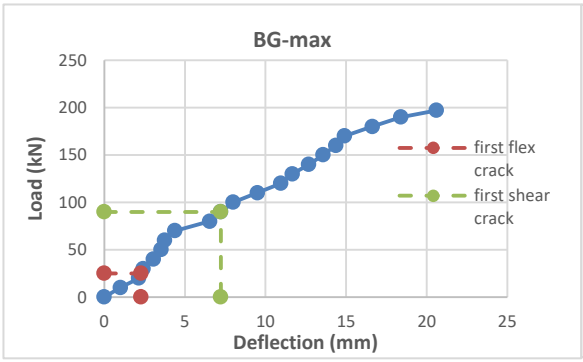


**Fig 10.** Load- deflection curve in mid span for BG-max

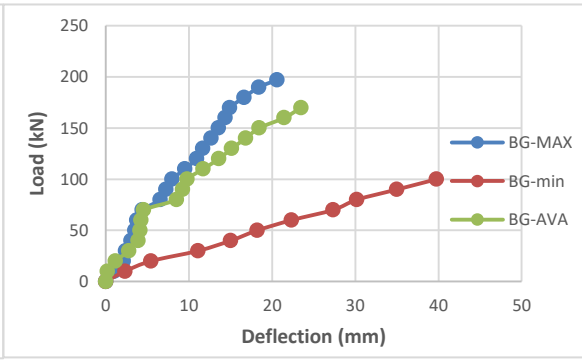


**Fig 11.** Load- mid span deflection for all specimen

### 3.3 Strain Measurements

In order to understand the behavior of the reinforced concrete box girders with different main longitudinal reinforcement ratios, it is necessary to know the values of the strain in the concrete, at the top surface of the three box specimens. In addition, knowing the strain values in the reinforcement, in the center of the main longitudinal reinforcement in addition to the shear reinforcement near the supports, Figs. 12 and13. In the following two subsections, the most important strain readings are reviewed, along with discussions related to them.

*3.3.1 Average Concrete Surface Strains. As seen in Figs. 12 and 13, the upper faces of the three beams suffered from an increase in the strain readings directly proportional to the amount of the main reinforcement, that is, the higher the main reinforcement, the higher the compressive strain readings in the upper faces of the three beams. It was also seen that the three beams did not have a compressive flexural failure, especially in the BG-min and BG-avr beams, which failed in tensile flexure. As for BG-max, it also did not experience compressive flexural failure in its upper face because the failure occurred near the supports, i.e., it was a shear failure.*

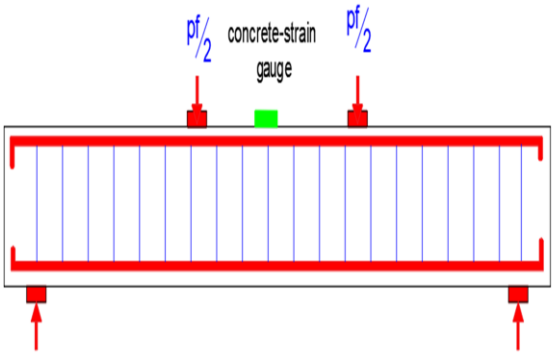


**Fig 12.** Concrete-Strain gauge location for the three specimens

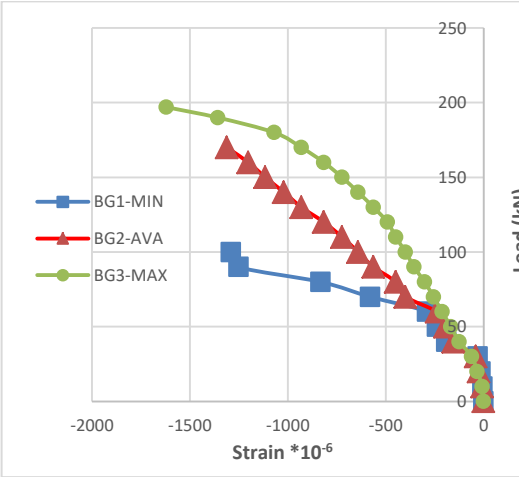


**Fig 13**. Applied load versus average compression strain in concrete for the three specimens

### 3.4. Steel Reinforcement Strain Values

Four steel strain gauges were placed in each of the three box specimens; two horizontally at the middle of the main steel reinforcement (main) and two vertical (VR and VL) at the shear steel reinforcement (stirrups) near the supports, Fig. 14. All the three steel strain gauges read increases in strain values associated with an increase in the values of the applied loads to failure. In more detail, the main reinforcing steel in BG-min and BG-avr reached yield, Figs. 15 and 16, while the stirrup shear steel in them did not reach yield. As for BG-max, the main steel reinforcement did not reach the yield, Fig. 17, but the stirrup shear steel did reach yield. This explains the mode of failure that occurred in the three specimens, which is the failure of ductile flexure in BG-min & BG-avr, besides the brittle shear failure in BG-max.

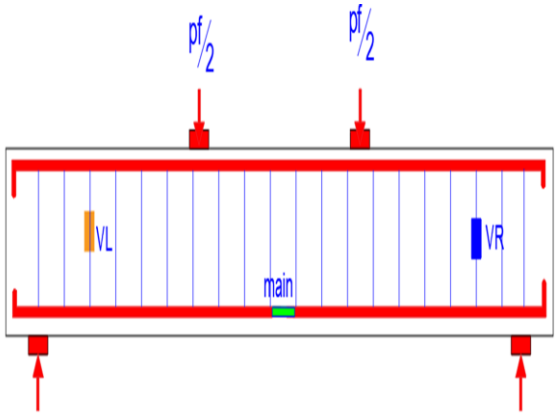


**Fig 14.** Steel-Strain gauge location for the three specimens

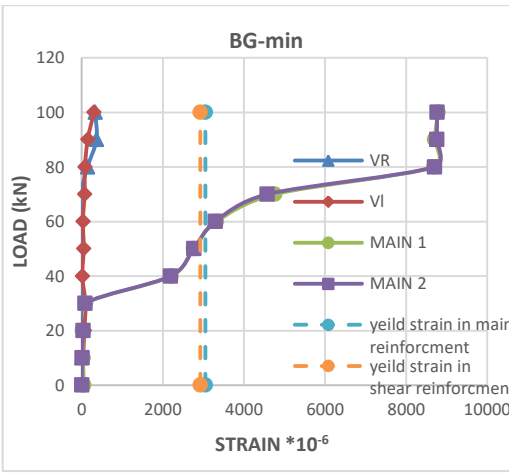


**Fig 15.** Applied Load versus steel reinforcement in BG-min

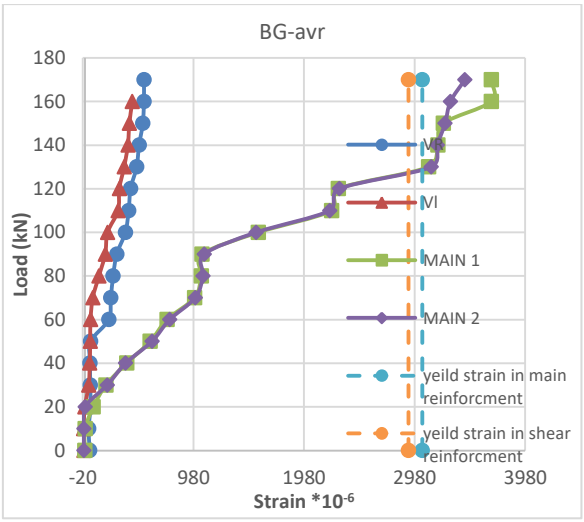


**Fig 16.** Applied load versus steel reinforcement in BG-avr

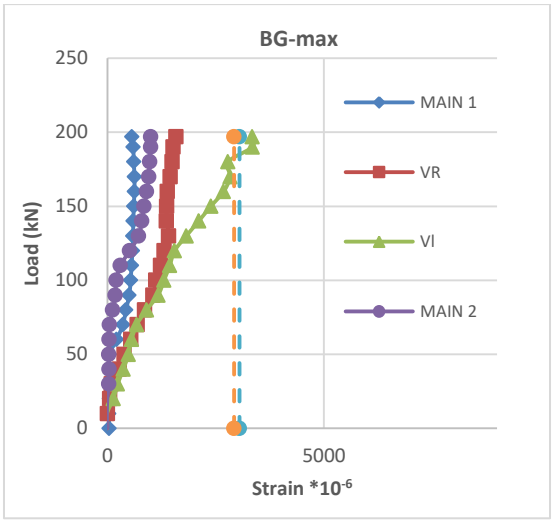


**Fig 17.** Applied load versus steel reinforcement in BG-max

## 4. DISCUSSION OF THE RESULTS

For accuracy, the results can be discussed in the form of the following points:

Through the results of the tests, it is seen that the load at which the fist flexural crack occurred was 30 kN, 27 kN and 25 kN for BG-min, BG-avr and BG-max, respectively. That is, they are remarkably close, due to the unification of the cross-sectional dimensions and concrete properties of the three specimens. However, after the appearance of flexural cracks in all three specimens, the main reinforcing steel began to directly participate in the load resistance of the concrete, which was reflected in the values of the load at which the first shear crack appeared in the three specimens. In more detail, the first shear crack appeared at 65 kN, 80 kN and 90 kN for BG-min, BG-avr and BG-max, respectively.

When using the ratio of minimum main reinforcement in BG-min, the failure was flexure, because the main reinforcement reached the yield at 99 kN load, while the secondary reinforcement (shear reinforcement) was far from the yield at this load. In the case of using the average of main reinforcing steel in BG-avr, the failure was flexural failure as well, but with 66% more load capacity than BG-min. This is due to the capacity than BG-min. This is due to the fact that the resistance to bending stresses increases at a high rate with the increase of the main reinforcement. In more detail, the secondary reinforcement reaches yielding before the main reinforcement does, causing shear failure.

The deflection increased linearly with load increment during the pre-cracking stage. This was expected because the strain values in steel and concrete are relatively small, both materials are in the elastic portion of their respective responses. From 30.3% (for BG-min), 16.45% (for BG-avr) to 12.6% (for BG-max) of the final load capacity, initial cracking was observed.

The effective moment of inertia of the beam cross section decreases in the post-cracking stage when concrete cracking alters the slope of the load-deflection curve. Up until the point at which the tensile steel begins to yield, the deflection values increased once more almost linearly with the increase in load after the crack. A change in the slope of the load-deflection curve and a decrease in stiffness were two characteristics of this stage.

All load-deflection response curves change in slope during the post-yielding stage took place as a result of the tensile longitudinal steel reinforcement yielding. Due to the decrease in neutral axis depth after yielding, the deflections immediately increased.

## 5. SUMMARY RELATIONSHIPS

The Figures 18 and 19 show the load capacity-reinforcement ratio and midspan deflection-reinforcement ratio relationships, respectively. The relationships below can be safe, useful and quick to use by structural engineers.

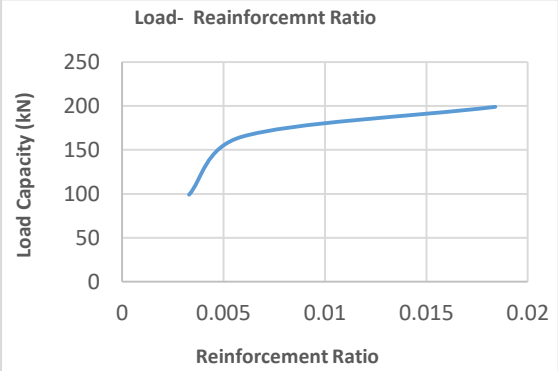


**Fig 18.** Load capacity versus main reinforcement ratio

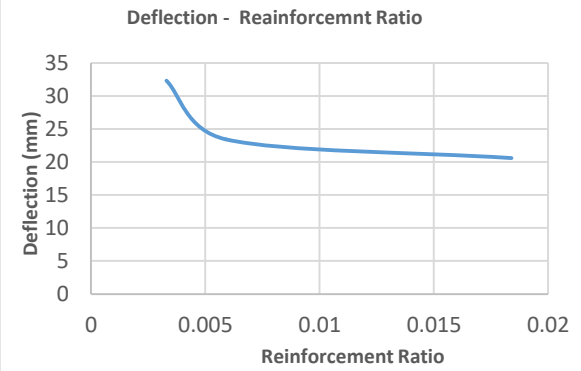


**Fig 19.** Midspan deflection versus main reinforcement ratio

## 6. CONCLUSION

When reinforcing the first box girder (BG-min) with the ACI 318-19 minimum main longitudinal reinforcement ratio ($\rho_{min}$), the region of maximum flexural stresses (the region between the two applied forces) is the one that clearly witnessed deformations, because it is weaker than the regions of maximum shear stresses (the regions between the applied forces and the supporting reactions). When reinforcing the second box girder (BG-avr) with average main longitudinal reinforcement ratio ($\rho_{avr}$), it did not change much, as the region of maximum flexural stresses remained the one subjected to the highest deformations because it remained weaker than the shear regions. On the other hand, when the reinforcement ratio was increased to the ACI 318-19 maximum main longitudinal reinforcement ratio ($\rho_{max}$) in the third box girder (BG-max), the zone of maximum flexural stresses became stronger than the shear zones, and thus forced the failure to change its location from the middle of the box (as in BG-min and BG-avr specimens) to the shear zones near the supports. Accordingly, the most important conclusions can be summarized in the following points:

In reinforced concrete box girders, increasing the ratio of main reinforcing steel to 79%, which is the average reinforcing steel between the maximum and minimum values of the ACI 318-19, and to 456%, which is the maximum value of the main reinforcing steel according to the ACI 318-19, led to an increase in load capacity by 66% to 99%, respectively, although the failure mode differs. This also led to a decrease in the values of maximum deflection in the middle of the spans to about 28% and 36%, respectively.

Steel reinforcement yield occurred at both minimum and average main reinforcement resulting in flexural failure. While at the maximum of the main reinforcement, yield did not urge but rather a failure occurred in another place which is the shear, whose stirrups suffered from yield this time. If this indicates something, it indicates that the ACI 318-19 code covers all the ranges of the main reinforcement efficiently from the minimum value to the maximum one.

When the main reinforcement is the minimum, average, and maximum, the first cracks to appear are the flexural cracks, at 30%, 16% and 12% of the load capacity, respectively. Then, that is, immediately after the appearance of the first cracks, the main reinforcing steel begins to participate in the load resistance directly, which leads to the appearance of shear cracks at 65%, 48% and 45% of the load capacity, respectively as well.

When the main reinforcement is minimum, average, and maximum, the relationship of load to midspan deflection remains linear until the appearance of flexural cracks. If the reinforcing ratio is the minimum and average, the curvature begins to appear on this relationship, this curvature continues until the ductile flexural failure occurs. On the other hand, if the main reinforcement is the maximum,

the straight nature of the load-deflection relationship remains continuous, until the appearance of shear cracks, and even after that, it remains straight until the brittle shear failure occurs.

ACKNOWLEDGMENT
The authors would like to express their deepest thanks and gratitude to the Department of Civil Engineering\College of Engineering\University of Diyala for their support that contributed to the completion of the current research work.

## References

1. K. Hemalatha, C. James, L. Natrayan, V. Swamynadh. “Analysis of RCC T-beam and prestressed concrete box girder bridges super structure under different span conditions,” Materials Today Proceedings, 2021, 37, pp.1507-1516.
2. R. Thakai, R. Deshpande and S. Bedkihal, “Parametric Study on Behavior of Box-Girder Bridges Using Finite Element Method,” 2016.
3. R. A. miller, G. M. Hlavacs, T. Long and A. Greuel, “Full-scale testing of shear keys for adjacent box girder bridge,” PCI journal, 1999, 44, pp. 6.
4. K. Hanna, G. Morcous, and M. Tadros, “Design detailing, and testing of non-post-tensioned transverse connections in adjacent box-girder bridges,” PCI J, 2011, 56, pp. 94-107.
5. AASHTO LRFD Bridge design specifications, Washington, DC, 2017.
6. American Concrete Institute and International Organization for Standardization. “Building code requirements for structural concrete (ACI 318-19) and commentary,” 2019.
7. T. L. WANG, and D. Huang, “Vehicle impact in box girder bridges and bridge substructures,” 1994, FL/DOT/RMC, pp. 0696-8677.
8. P. Agarwal, P. Pal, and P. K. Mehta, “Parametric study on skew-curved RC box-girder bridges,” Elsevier, December, 2020, V. 28, pp. 380-388.
9. K. K. Bhagwat, D. K. Kulkarni and P. Cholappanavar, “Parametric study on behaviour of box girder bridges using CSi Bridge,” International Research Journal of Engineering and Technology (IRJET), 2017, V. 4.
10. P. K. Gupta, K. K. Singh and A. Mishra, “Parametric study on behaviors of box-girder bridges using finite element method,” Asian Journal of Civil Engineering (Building and Housing), 2010.
11. C. Yilmaz, “Ultimate strength of box girders by finite element method,” PhD, thesis, 1975.
12. M. Hassanain, “Design of adjacent precast box girder bridges according to aashto lrfd specifications,” in Short & Medium Span,” In 6th International Conference on Short & Medium Span Bridges, Bridge Engineering, CSCE, Vancouver, 2002.
13. J. Wang, S. Tang, H. Zheng, C. Zhou and M. Zhu, “Flexural behavior of a 30-meter full-scale simply supported prestressed concrete box girder,” Applied Sciences, 2020, 10 (9), pp. 3076.
14. A. Mohammed, K. S. Abdul-Razzaq, R. D. Khalaf and A. K Hussein, “Suggesting deflection expressions for RC beams,” International Journal of Civil Engineering and Technology, 2019, 10 (3).
15. K. S. Abdul-Razzaq, A. H. Mohammed and T. K. Mohammedali, Suggesting deflection expressions for RC 2-way slabs,” International Journal of Civil Engineering and Technology, 2019, 10 (2).
16. Iraqi Specification No. 5. “Portland cement. Iraqi Central Agency for Standardization and Quality Control,” translated from Arabic edition, 1984.
17. Iraqi Specification No. 45. “Aggregate from natural sources for concrete,” Iraqi Central Agency for Standardization and Quality Control, translated from Arabic edition, 1984.
18. ASTM A496-02, “Standard specification for steel wire, deformed, for concrete reinforcement,” ASTM Committee A-1 on steel, stainless steel, and related alloys, West. Conshohocken, PA 19428-2959, United States 2002, pp. 5.
19. ASTM A615/A615M-05, “Standard specification for deformed and plain carbon-steel bars for concrete reinforcement,” ASTM Committee A-1 on Steel, Stainless Steel, and Related Alloys, West Conshohocken, United States 2005, 5, pp. 19428-2959,
20. ASTM C496. “Standard specification for splitting tensile strength of cylindrical concrete specimens,” Philadelphia, PA: American Society for Testing and Materials, 1996.

21. ASTM C39. “Standard specification for testing method for compressive strength of cylindrical concrete specimens,” *Philadelphia, PA: American Society for Testing and Materials*, 2003.
22. ASTM C78. “Standard test method for flexural strength of concrete (using simple beam with third-point loading,” *Philadelphia, PA: American Society for Testing and Materials*, 2002.